Available online at www.sciencedirect.com
SCIENCE DIRECT®
Chemical Physics Letters 382 (2003) 133–141
CHEMICAL PHYSICS LETTERS
www.elsevier.com/locate/cplett

Carbon nanotube fracture – differences between quantum mechanical mechanisms and those of empirical potentials

Diego Troya, Steven L. Mielke, George C. Schatz *

Department of Chemistry, Northwestern University, Evanston, IL 60208-3113, USA

Received 2 October 2003; in final form 2 October 2003
Published online: 6 November 2003

Abstract

We present quantum mechanical (QM) studies of carbon nanotube (CNT) fracture using two different semiempirical methods. One proposed mechanism for CNT fracture – based mainly on studies with empirical potentials – involves an aggregation of Stone–Wales defects followed by a ring-opening step whereby a bond between two 5-membered rings is severed. We have performed QM studies which instead predict that this bond is a particularly strong one, and that the failing bonds lie *within* the pentagons. We also explore why empirical bond-order potentials (in particular, a potential of Brenner and coworkers) predict qualitatively different fracture mechanisms than quantum mechanical calculations do.

1. Introduction

Due to their excellent mechanical properties, carbon nanotubes (CNTs) have been the subject of intense interest as nanoreinforcements for use in a variety of composites. A number of studies, both theoretical [1–18] and experimental [1,19–25], have been performed to understand the mechanical properties and failure mechanisms of isolated CNTs under axial tension (we caution the reader that the references we have given here are intended to be representative rather than comprehensive, for a more extensive review see Qian et al. [26]). Defects, either those introduced during the CNT synthesis or stress induced ones, play a central role in most of the proposed failure mechanisms. In particular, the Stone–Wales (SW) defect [27], i.e., the result of a bond rotation that transforms 4 hexagons into 2 pentagons and 2 heptagons, has received the most attention. Calculations [5,11] have shown that the formation of a SW defect becomes energetically favorable at strains above about 5% (for a [5,5] armchair tube) although the barrier to defect formation remains quite high.

Simulations have also shown [4,16] that SW defects can – at least at high temperatures – bifurcate and migrate along the tube, and furthermore that defect aggregation becomes energetically favorable at high strains [4]. Yakobson [6] has proposed that after several SW defects have migrated together fracture can be initiated via a

* Corresponding author. Fax: +1-18474917713.
E-mail address: schatz@chem.northwestern.edu (G.C. Schatz).

0009-2614/$ - see front matter © 2003 Elsevier B.V. All rights reserved.
doi:10.1016/j.cplett.2003.10.068

mechanism whereby a bond connecting two pentagon rings is severed – resulting in the formation of larger rings, which ultimately leads to CNT yielding. Yakobson reported no explicit calculations to support this mechanism, but calculations have been reported by others that show the bond between two pentagon rings failing [13].

Most of the early theoretical investigations of CNTs have relied on the empirical potentials of Brenner and co-workers [28,29] which are based on earlier work by Tersoff [30] using the bond-order scheme of Abell [31], but other, more ad hoc, empirical potentials have also been used [3,13]. These empirical potentials have had considerable success at obtaining semiquantitative results for many properties of carbon nanotubes, but caution should be used in their application to investigate details of CNTs which were not included in their parametrization. Therefore, where feasible, the performance of these potentials is best validated against results obtained via tight-binding, semi-empirical, or density functional theories.

We have recently begun modeling CNT fracture using quantum mechanical methods (both semi-empirical and density functional theory) and we find that the bonds connecting two pentagon rings are especially strong, and it is other bonds that fail in fracture events – even when this requires the fracture of up to twice as many bonds. Thus, the specific details of the ring-opening mechanism proposed by Yakobson must be modified.

2. Theory

The semiempirical quantum mechanical calculations reported here used the MSINDO [32] and PM3 methods [33]. In this initial study, we confine our attention to [5,5] armchair nanotubes with 0, 1, 2, or 5 adjacent SW defects. We employ open-ended tubes consisting of 170 carbon atoms and which are capped at the ends by hydrogen atoms. Restricted Hartree–Fock (RHF) wavefunctions are used throughout, after verifying invariance of results with respect to open shell unrestricted semiempirical calculations.

Fig. 1 displays the unstrained structures of a [5,5] pristine tube (a), and [5,5] tubes with 1 (b), 2 (c), and 5 (d) adjacent SW defects in which the pentagon–pentagon bonds are axially aligned.

We also investigate the ability of the second generation reactive empirical bond-order potential of Brenner and co-workers [29] to model CNT fracture events. It has already been noted that the cutoff function used to truncate the bond-order potentials of Brenner and co-workers to nearest-neighbor interactions (all three versions of this potential use the same cutoff function which begins at 1.7 Å and completely damps out interactions at separations beyond 2.0 Å) can produce spurious results [13,34]. We will consider simulations with the latest published version of the potential (which we will denote TB-G2) as well as a modified potential (which we will denote MTB-G2) using a procedure originally suggested by Shenderova et al. [34] which removes the cutoff function while only including interactions between pairs of carbon atoms that are *initially* within a 2 Å distance in the original unstrained structure (operationally this is achieved by never updating the initial neighbor list). This approach does not allow the formation of new bonds, but for the specific case of modeling the stretching of CNTs via axial tension this may be an acceptable approximation.

The PM3 and MSINDO geometry optimizations reported in this work took roughly three orders of magnitude more CPU time than the TB-G2 or MTB-G2 optimizations, so the QM calculations were performed at a limited number of strain values. Typically, we performed optimizations at strain increments of 0.5% until the tubes failed. We fixed the plane of hydrogen atoms and the neighboring carbon atoms while stretching the tubes so that the distances between these atoms are those of the unstrained configurations. Strain is applied by increasing the axial distance between the frozen planes of carbon atoms at the two edges of the tubes. We note that both the failure strain and stress at failure depend somewhat on the manner in which the strain is incremented, as close to failure there are multiple paths for fracture. This is especially true of the PM3 results, where structures having larger failure strains than we present below were obtained with a different algorithm. However the magnitudes of these variations are not sufficient to affect our conclusions

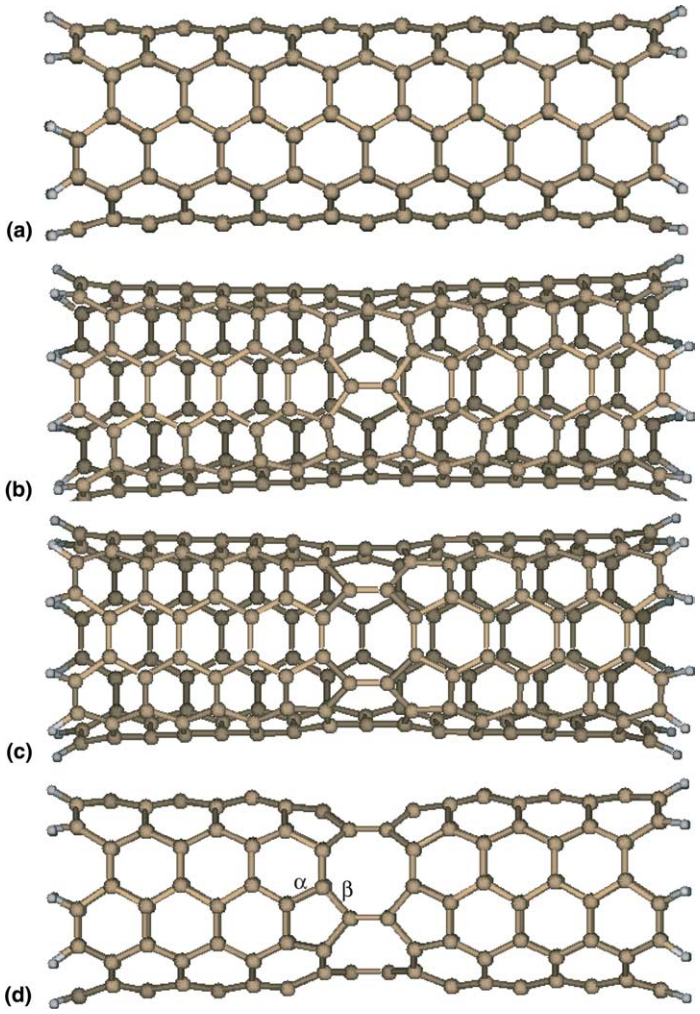

Fig. 1. Equilibrium structures of the [5,5] nanotubes included in this study: (a) pristine (defect free), (b) 1 defect, (c) 2 adjacent defects, (d) 5 adjacent defects. α and β denote the two types of C–C bonds axially aligned within the pentagons.

about fracture mechanisms, so all the results will refer to the algorithm described above.

3. Calculations and discussion

We begin by presenting the behavior under strain of a [5,5] CNT with 5 adjacent SW defects with pentagon–pentagon bonds axially aligned (Fig. 1d). Fig. 2 shows the evolution of C–C internuclear distances from the edge to the center of the nanotube, (where the SW defects are), as a function of the applied strain. Note that we only plot half of the overall C–C bonds since the other half are equivalent by symmetry. Panel (a) shows the results for the unmodified Brenner potential (TB-G2), panel (b) is for MTB-G2 and panel (c) is for the PM3 semiempirical results. The MSINDO results are omitted here, but they are analogous to those of PM3. Fig. 2a illustrates why the original cutoff function in the TB-G2 potential is not appropriate when treating nanotube fracture. At zero strain, most of the C–C internuclear bond lengths along the tube are of similar magnitude. Only the

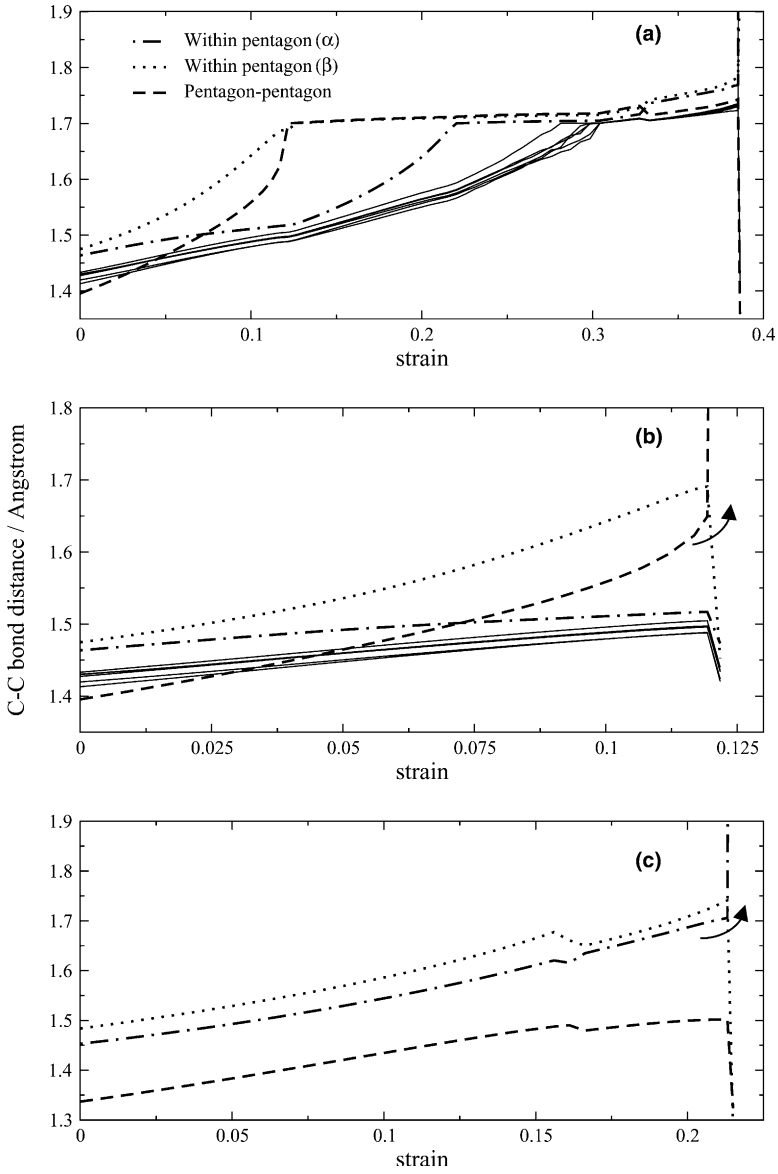

Fig. 2. Calculated C–C internuclear bond distances along a row of carbon atoms in a [5,5] CNT with 5 Stone–Wales defects as a function of strain for different potential energy methods: (a) TB-G2, (b) MTB-G2, (c) PM3. See Fig. 1 for definition of α and β. The solid lines in (a) and (b) indicate distances for C–C bonds further removed from the defect site and have been omitted from (c) for clarity.

pentagon–pentagon bonds (which are slightly shorter) and the bonds within the pentagons (which are slightly longer) show deviations from the average C–C internuclear bond distance. Upon axial tension, the C–C bond lengths increase at different rates. An anomaly associated with the cutoff function is observed by noting that a C–C bond distance which reaches $\sim$1.7 Å undergoes only very slight additional elongation until all of the strained C–C bond distances along the tube reach $\sim$1.7 Å. This results from a spurious force in the TB-G2 potential that is switched on for

distances larger than 1.7 Å by the cutoff function, and which has been characterized earlier (see Fig. 1 of Belytschko et al. [13]). At large strain values, where the effects of the cutoff function become significant, the radius of the tube contracts at an abnormally high rate since elongation of the tube via angular distortions becomes preferable to elongation via further bond-length stretching. Eventually, the distances between next-nearest neighbors can drop below the 2 Å cutoff distance and anomalous coordination changes occur, leading to an unphysical failure mechanism.

The results of the MTB-G2 potential are shown in Fig. 2b. At moderate strain (below ~25% for the case of the undefected tube) these are identical to those of TB-G2; however, the elongation and breakage pattern is substantially different. The MTB-G2 tube fails at much smaller strains than those observed with TB-G2. The pentagon–pentagon bonds are the ones that fail even though they are not the most stretched bonds until just prior to failure. Fig. 2c shows that the PM3 results do not follow this trend. At zero strain, the pentagon–pentagon bonds (1.34 Å) in both PM3 and MSINDO calculations are noticeably shorter than the rest of the bonds. In clear contrast with the results of the two bond-order potentials, the rate of increase in the internuclear distance with strain of this bond is much lower than that of the rest of the bond distances, and several bonds other than the pentagon–pentagon fail, including bonds within the pentagons. These findings are particularly interesting since in this tube containing 5 adjacent SW defects, breakage of the tube along the pentagon–pentagon seam, as in the case of the MTB-G2 potential, would require failure of only 5 bonds, whereas failure elsewhere implies breaking twice as many bonds. We have verified the generality of this trend by stretching other tubes containing a single SW defect (Fig. 1b) and 2 defects (Fig. 1c). As we have noted in the case of the TB-G2 potential in the 5 SW defected tube, although there are distances which at low strains stretch at a larger rate than others, those bonds do not keep stretching after reaching ~1.7 Å. When all of the internuclear distances are ~1.7 Å, a somewhat uniform elongation of all of the bonds is observed until failure occurs. Removing the cutoff function (MTB-G2 potential) avoids the unphysical evolution of the C–C internuclear bond distances that are 1.7 Å or larger. However, the modified potential predicts that breaking the pentagon–pentagon bonds is the lowest energy process. In both PM3 and MSINDO calculations, the shortest distance corresponds to the bonds between pentagons in all SW defected tubes. The longest distances are those within the pentagons, which elongate at a higher rate and are ultimately responsible for the tube failure.

We note that the bond distances displayed in Fig. 2 correspond to a single row (of the 10 rows present in a [5,5] CNT) of C–C bonds along the axial dimension of the nanotube. Since bond strength is inversely proportional to bond length, we can predict the relative strengths of various bonds based on their lengths; this concept will be used in some of the analysis presented below.

To gain deeper insight into the mechanism of CNT failure, we show in Fig. 3 schematic unrolled representations of the defected region of the five-fold SW defected tube at strains just below failure as predicted by the four different interaction potentials considered here. In the PM3 and MSINDO calculations it can be clearly seen that the pentagon–pentagon bonds are the stronger ones while bonds within the pentagons are noticeably weaker. In the MTB-G2 calculations, we also see that one of the weakest sets of bonds is that corresponding to the heptagon bonds that are aligned along the strain axis. However, the bonds within the pentagon are about as strong as those between pentagons and the tube ultimately prefers to yield by breaking the pentagon–pentagon bonds. MTB-G2 predicts that the bonds between pentagons weaken more rapidly close to fracture than other bonds in the defect. As a result, fracture involves breakage of only the five bonds between the pentagons. This is in stark contrast to our quantum mechanical results where breakage of roughly twice as many strong bonds is needed for fracture, as we shall see later.

These findings give evidence of flaws in the widely used empirical bond-order potentials regarding CNT fracture mechanisms. As previously discussed, ring-opening mechanisms involving failure of pentagon–pentagon bonds have been

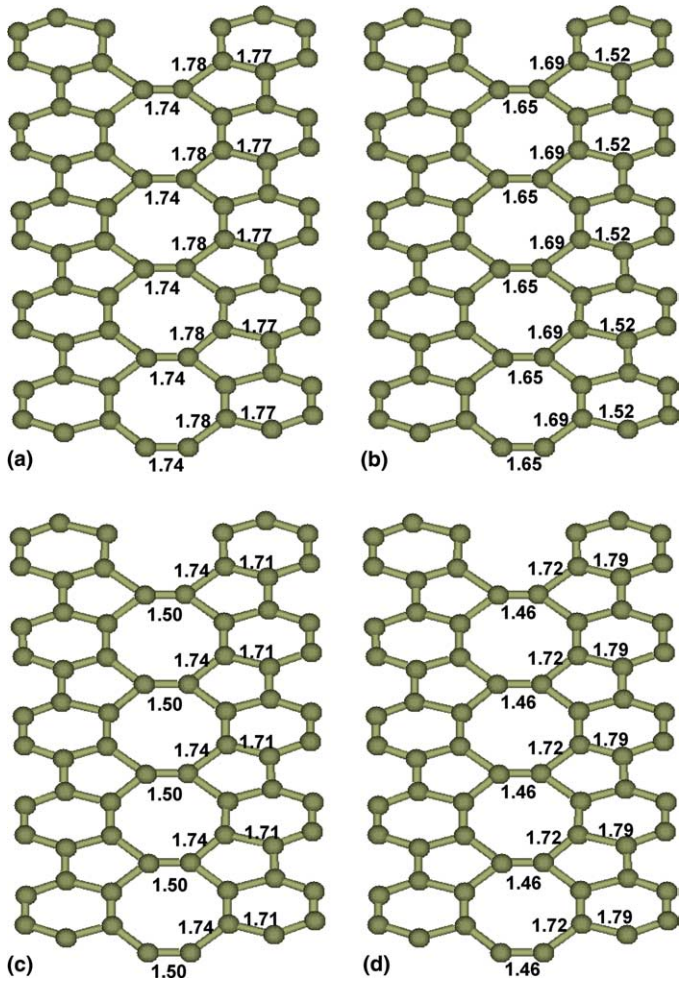

Fig. 3. Schematic representation of the defect region for a [5,5] CNT including 5 adjacent Stone–Wales defects in the step prior to failure. Internuclear distances are in Angstroms. Panels display results for: (a) TB-G2, (b) MTB-G2, (c) PM3 and (d) MSINDO, respectively. The strains of the displayed structures are: (a) 0.385, (b) 0.119, (c) 0.214 (d) 0.266.

invoked [6] to explain fracture processes in CNTs. To better understand which bonds fail first and initiate the fracture process, we have carried out molecular dynamics simulations using both PM3 and MSINDO. Starting from the structures depicted in Figs. 3c and d, we stretched the tubes by an additional 1%, and sampled initial velocities of the atoms from a Maxwell–Boltzmann distribution at 300 K while keeping the hydrogen atoms and the neighboring planes of carbon atoms fixed. We let the system evolve in time integrating the equations of motion for 340 fs with steps of 0.2 fs. Fig. 4 shows the evolution of a fivefold SW defected tube at different times calculated using PM3 (the MSINDO results are similar). These calculations reveal that the initial bond failure, subsequently leading to fracture, does not involve bonds between pentagons, due to their remarkable strength. Other bonds fail first, including those within the pentagons, and particularly those that are aligned along the strain axis. Even in the advanced stages of fracture, when many bonds have failed, it can be seen that the pentagon–pentagon bonds have not been severed.

Failure strains calculated in the step prior to failure are reported in Table 1. For pristine tubes,

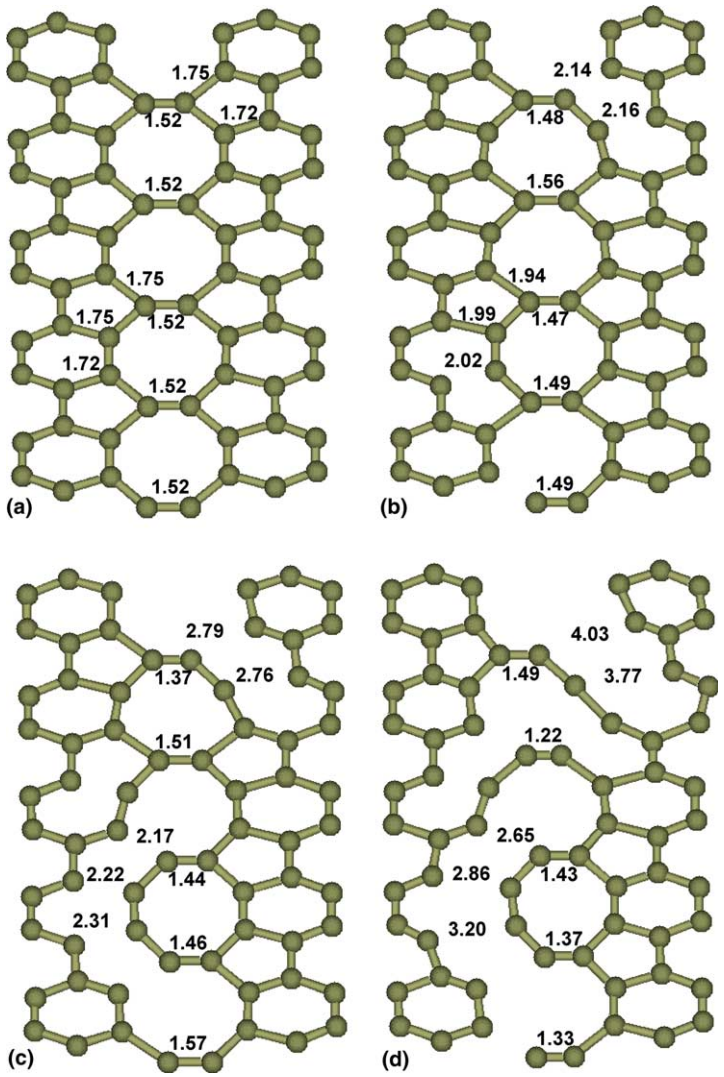

Fig. 4. Snapshots of a PM3 molecular dynamics simulation showing the defect region comprising 5 adjacent Stone–Wales defects of a [5,5] CNT (see text for details of the simulation). Times at which the snapshots are taken: (a) 0.0 fs, (b) 240 fs, (c) 300 fs and (d) 340 fs.

Table 1
Calculated failure strains of hydrogen-capped [5,5] carbon nanotubes with increasing number of adjacent Stone–Wales defects

	MSINDO	PM3	TB-G2	MTB-G2
[5,5] pristine	0.279	0.234	0.411	0.256
[5,5] 1 SW	0.244	0.221	0.395	0.162
[5,5] 2 SW	0.241	0.212	0.376	0.154
[5,5] 5 SW	0.266	0.214	0.385	0.119

calculations with TB-G2 show failure strains which are significantly higher than have been experimentally observed [24]. MTB-G2 predicts a failure strain for the pristine tube of ~24% which is in substantially better agreement with recent experimental [24] results (~30%), the PM3 (~23%) and MSINDO (~28%) results, and prior [18] AM1 (~23%) calculations. However, this potential predicts (incorrectly) that increasing the number of SW defects dramatically decreases both the failure strain and the stress at failure. For the case of five adjacent SW defects the MTB-G2 PES predicts a failure strain that is about half of what it predicts for the undefected tube; this would be reasonable if all the C–C bonds were of comparable strength, but it fails to account for the substantially greater strength of the pentagon–pentagon bonds. The strains at failure of defected nanotubes, as predicted by either of the semiempirical methods, are only slightly decreased from those of the pristine tubes and displayed no significant correlation with the number of defects.

The QM prediction that the introduction of SW defects – even large numbers of adjacent defects – results in only a minimal decrease in the strain at failure of CNTs is dramatically different than the role these defects are usually assumed to play. Several theories [6,12,15–17] have been proposed that predict the failure strain of CNTs as a function of temperature based on the assumption that the formation of SW defects is the rate-limiting step to fracture. At low-temperatures (e.g. 300 K) the high barrier to the formation of a SW defect makes such mechanisms questionable. At higher temperatures, SW defect formation clearly *does* cause weakening in simulations based on bond-order potentials, but quantum mechanically the remarkable strength of the pentagon–pentagon bonds compensates for the reduction in the number of bonds that need to be broken (at least in armchair CNTs), and restricts the formation of larger rings that can serve as nucleation sites for larger cracks. This result suggests that several estimates of nanotube failure [12,15–17] need to be reevaluated. It should be noted that in tubes with different chirality, the degree of alignment of the weak bonds described here with the tube axis will dictate the effect of defect formation on the nanotube failure mechanisms and mechanical properties.

We have also calculated the stresses in the step prior to failure for the pristine tube, assuming the shell thickness to be 3.4 Å. The TB-G2 results (347 GPa at 0.411 strain) are way above the rest of the results (103 GPa at 0.256 strain for MTB-G2, 130 GPa at 0.234 strain for PM3 and 163 GPa at 0.279 strain for MSINDO), further indicating the inability of this potential to describe failure properties. MSINDO seems to overestimate PM3 and MTB-G2.

Calculations of the Young's modulus of the [5,5] defect-free nanotube also point out differences in the potential energy methods used in this work. The Young's moduli of the TB-G2 and MTB-G2 potentials are both fairly low at 0.82 TPa (since the cutoff function does not affect TB-G2 at low strains the two results are identical). MSINDO predicts a significantly larger Young's modulus of 1.40 TPa, while PM3 gives a more reasonable value of 1.16 TPa. These results may be compared with the DFT results of Hernández et al. [7] which predicted a modulus of 1.09 TPa for a [6,6] CNT and with the known value of graphene of 1.06 TPa.

4. Concluding remarks

We have demonstrated that some empirical potentials do a poor job of reproducing the qualitative features of carbon nanotube fracture under axial tension and have suggested that quantum calculations may be required to treat such events accurately. In particular, we showed that certain details of a previously proposed ring-opening fracture mechanism [6] are not reproduced by quantum calculations. More generally, we show that the bonds connecting two pentagon rings are much stronger than empirical bond-order potentials predict, and thus these bonds are not the weak link that permits the nucleation of cracks in aggregations of Stone–Wales defects. Instead, the failing bonds are observed to include those that lie within the pentagon rings – even though this necessitates the fracture of a greater number of bonds. We have also shown that certain mechan-

ical properties of carbon nanotubes, as predicted by the widely used empirical bond-order potentials, are in disagreement with those predicted by more rigorous semiempirical quantum mechanical methods. Bond-order potentials have also recently been shown to do a poor job of predicting the energy ordering of fullerene isomers, in part because they underestimate the instability of adjacent pentagon rings [35]. These failures may motivate continued revision of the empirical potentials.

Acknowledgements

We gratefully acknowledge the grant support from the NASA University Research, Engineering and Technology Institute on Bio Inspired Materials (BIMat) under award No. NCC-1-02037.

References

[1] S. Iijima, C. Brabec, A. Maiti, J. Bernholc, J. Chem. Phys. 104 (1996) 2089.
[2] B.I. Yakobson, C.J. Brabec, J. Bernholc, Phys. Rev. Lett. 76 (1996) 2511.
[3] J.P. Lu, Phys. Rev. Lett. 79 (1997) 1297.
[4] M.B. Nardelli, B.I. Yakobson, J. Bernholc, Phys. Rev. Lett. 81 (1998) 4656.
[5] M.B. Nardelli, B.I. Yakobson, J. Bernholc, Phys. Rev. B 57 (1998) R4277.
[6] B.I. Yakobson, Appl. Phys. Lett. 72 (1998) 918.
[7] E. Hernández, C. Goze, P. Bernier, A. Rubio, Phys. Rev. Lett. 80 (1998) 4502.
[8] P. Zhang, P.E. Lammert, V.H. Crespi, Phys. Rev. Lett. 81 (1998) 5346.
[9] D. Sanchez-Portal, E. Artacho, J.M. Soler, A. Rubio, P. Ordejon, Phys. Rev. B 59 (1999) 12678.
[10] P. Jensen, J. Gale, X. Blase, Phys. Rev. B 66 (2002) 193403.
[11] Q. Zhao, M.B. Nardelli, J. Bernholc, Phys. Rev. B 65 (2002) 144105.
[12] G.G. Samsonidze, G.G. Samsonidze, B.I. Yakobson, Phys. Rev. Lett. 88 (2002) 065501.
[13] T. Belytschko, S.P. Xiao, G.C. Schatz, R.S. Ruoff, Phys. Rev. B 65 (2002) 235430.
[14] T. Xiao, K. Liao, Phys. Rev. B 66 (2002) 153407.
[15] G.G. Samsonidze, G.G. Samsonidze, B.I. Yakobson, Comput. Mater. Sci. 23 (2002) 62.
[16] C. Wei, K. Cho, D. Srivastava, Phys. Rev. B 67 (2003) 115407.
[17] C. Wei, K. Cho, D. Srivastava, Appl. Phys. Lett. 82 (2003) 2512.
[18] T. Dumitrica, T. Belytschko, B.I. Yakobson, J. Chem. Phys. 118 (2003) 9485;
J. Chem. Phys. 119 (2003) 1281E.
[19] P. Poncharal, Z.L. Wang, D. Ugarte, W.A. de Heer, Science 283 (1999) 1513.
[20] D.A. Walters, L.M. Ericson, M.J. Casavant, J. Liu, D.T. Colbert, K.A. Smith, R.E. Smalley, Appl. Phys. Lett. 74 (1999) 3803.
[21] M.-F. Yu, B.S. Files, S. Arepalli, R.S. Ruoff, Phys. Rev. Lett. 84 (2000) 5552.
[22] M.-F. Yu, O. Lourie, M.J. Dyer, K. Moloni, T.F. Kelly, R.S. Ruoff, Science 287 (2000) 637.
[23] B.G. Demczyk, Y.M. Wang, J. Cumings, M. Hetman, W. Han, A. Zettl, R.O. Ritchie, Mater. Sci. Eng. A 334 (2002) 173.
[24] D. Bozovic, M. Bockrath, J.H. Hafner, C.M. Lieber, H. Park, M. Tinkham, Phys. Rev. B 67 (2003) 033407.
[25] H.E. Troiani, M. Miki-Yoshida, G.A. Camacho-Bragado, M.A.L. Marques, A. Rubio, J.A. Ascencio, M. Jose-Yacaman, Nano Lett. 3 (2003) 751.
[26] D. Qian, G.J. Wagner, W.K. Liu, M.-F. Yu, R.S. Ruoff, Appl. Mech. Rev. 55 (2002) 495.
[27] A.J. Stone, D.J. Wales, Chem. Phys. Lett. 128 (1986) 501.
[28] D.W. Brenner, Phys. Rev. B 42 (1990) 9458;
Phys. Rev. 46 (1992) 1948E.
[29] D.W. Brenner, O. Shenderova, J. Harrison, S. Stuart, B. Ni, S. Sinnott, J. Phys.: Condens. Matter 14 (2002) 783.
[30] J. Tersoff, Phys. Rev. Lett. 61 (1988) 2879.
[31] G.C. Abell, Phys. Rev. B 31 (1985) 6184.
[32] B. Ahlswede, K. Jug, J. Comp. Chem. 20 (1999) 563.
[33] J.J.P. Stewart, J. Comp. Chem. 10 (1989) 209.
[34] O.A. Shenderova, D.W. Brenner, A. Omeltchenko, X. Su, L.H. Yang, Phys. Rev. B 61 (2000) 3877.
[35] E. Albertazzi, C. Domene, P.W. Fowler, T. Heine, G. Seifert, C.V. Alsenoyd, F. Zerbettoe, Phys. Chem. Chem. Phys. 1 (1999) 2913.